THE ASTROPHYSICAL JOURNAL, 335:774–785, 1988 December 15

NEUTRAL ATOMIC CARBON IN DENSE MOLECULAR CLOUDS

J. ZMUIDZINAS, A. L. BETZ, R. T. BOREIKO, AND D. M. GOLDHABER
Space Sciences Laboratory, University of California
Received 1988 March 21; accepted 1988 June 7

ABSTRACT

We have detected the 370 μm $^3P_2$–$^3P_1$ fine-structure line of neutral carbon (C I) in seven sources: OMC 1, NGC 2024, S140, W3, DR 21, M17, and W51. Simultaneous analysis of our $J = 2$–1 data and available observations of the $J = 1$–0 line allow us to deduce optical depths and excitation temperatures for these lines. These data indicate that both C I lines are likely to be optically thin, and that the ratio of C I to CO column densities in these clouds is typically $\sim$0.1. The $J = 2$–1 [C I] line in the Orion BN/KL region shows no definite signs of emission from broad high-velocity line wings, such as those seen in CO. A comparison of $J = 2$–1 [C I] and CO(2–1) spectra provides an upper limit of 0.12 for the C I/CO column density ratio in the high-velocity gas. This limit, while more restrictive than those previously derived, does not indicate a depletion of C I relative to CO in the high-velocity gas, given the results of our observations of quiescent clouds.

Subject headings: infrared: spectra — interstellar: abundances — interstellar: molecules — nebulae: general

I. INTRODUCTION

Neutral atomic carbon (C I) has two fine-structure transitions in its electronic ground state: the $^3P_2$–$^3P_1$ transition at 809.3432 GHz (370.4145 μm) and the $^3P_1$–$^3P_0$ transition at 492.1612 GHz (609.1347 μm) (Cooksy *et al.* 1986). Recent advances in receiver technology have made it possible to observe these lines, allowing the abundance and excitation of C I in dense portions of the interstellar medium to be studied. The detection of the $J = 1$–0 line in dense molecular clouds was first reported by Phillips *et al.* (1980); additional observations were presented by Phillips and Huggins (1981). This line has also been mapped in one dimension across two clouds (M17 and S140) which have edge-on H II region-molecular cloud interfaces (Keene *et al.* 1985), and in the Orion molecular cloud (OMC 1) which has a face-on interface (Phillips and Huggins 1981). The observed $J = 1$–0 intensities implied large lower limits to the C I column densities ($N_{\rm CI} \sim 10^{18}$ cm^{-2} $\sim 0.1\ N_{\rm CO}$). Cloud chemistry models (Langer 1976*a*) predicted that C I should be abundant near the cloud surface due to the photodissociation of CO by interstellar ultraviolet radiation, but the predicted column densities were about one order of magnitude lower than those observed. In addition, the early time-dependent chemical models (Langer 1976*b*) predicted that all but a small fraction ($< 10^{-3}$) of C I initially present in the cloud interior would be converted to CO within 10^6 yr, a time scale which is short compared to cloud lifetime estimates. Later models were able to predict abundances more in line with C I observations (Graedel, Langer, and Frerking 1982; Tarafdar *et al.* 1985).

The $J = 1$–0 C I observations stimulated work on a number of models aimed at increasing the predicted amount of C I. A good review of these proposals is contained in Keene *et al.* (1985). As discussed in this review, the models fall into two general categories: (1) those which increase the C I produced in the photodissociation region near the cloud surfaces, such as the model described by Tielens and Hollenbach (1985*a*, *b*), and (2) those which increase the amount of carbon in the cloud interior, either through changes in the chemical network, through the production of UV photons in the cloud interior, through the sputtering of carbon from dust grains due to the passage of shock waves, or through an increase in the assumed C/O abundance. The observations of Keene *et al.* (1985) seem to rule out case (1) models, since the 492 GHz [C I] emission appears to be widespread throughout the clouds M17 and S140, and not localized near the interfaces between the molecular clouds and their associated H II regions (the interfaces are nearly perpendicular to the plane of the sky). On the other hand, UV photodissociation may be responsible for C I emission throughout the clouds if interior sources of UV radiation are available. For example, Stutzki *et al.* (1988) observe widespread low-level 158 μm [C II] emission in M17, as well as a peak near the interface region. In one interpretation, the extended [C II] emission component is a result of the UV radiation produced by a number of B-stars embedded in a clumpy cloud. The presence of C II directly demonstrates the presence of UV radiation, regardless of its source, and Stutzki *et al.* conclude that this UV could also be responsible for the extended [C I] emission observed.

Only lower limits to the C I column densities can be derived from [C I] 492 GHz observations alone, since the optical depth (and hence the excitation temperature) of the line is unknown, unless other assumptions are made. Phillips and Huggins (1981) have suggested that the optical depth of the 1–0 line for OMC-1 is $\tau_{10} \sim 25$, based on a comparison of [C I] and CO line widths, which implies that the C I excitation temperature is $T_x \sim 21$ K if the emission is spatially uniform. The resulting column density is $N_{\rm CI} \sim 3.5 \times 10^{19}$ cm^{-2} which gives $N_{\rm CI}/N_{\rm CO} \sim 0.7$. This large value is very difficult to understand theoretically, and almost certainly rules out models in which the C I is produced only in photodissociation regions. Alternatively, the C I column density and excitation temperature may be obtained directly by combining observations of both the $J = 2$–1 and $J = 1$–0 transitions, if the C I emission region does not have substantial temperature gradients.

The $^3P_2$–$^3P_1$ line was first detected by Jaffe *et al.* (1985) from ground-based observations of OMC 1. Unfortunately, large systematic and statistical uncertainties prevented Jaffe *et al.* from drawing firm conclusions from their data. To improve this situation, we have observed the 2–1 line with higher sensitivity in OMC 1 and six other clouds for which 1–0 data were

available, and have used the results from both lines to derive estimates for the line excitation temperatures and optical depths. Some of our results have already been presented (Zmuidzinas, Betz, and Goldhaber 1986, hereafter ZBG); here we extend that preliminary effort with an analysis of new $J = 2$–1 data for the sources OMC 1, NGC 2024, and S140, together with improved data for W3 and DR 21. In the tables that follow we have included our earlier results on W51 and M17 for completeness.

II. 809 GHz OBSERVATIONS

a) *Procedure*

Observations of the 809 GHz $^3P_2$–$^3P_1$ line of C I were performed over two flight series on the NASA Kuiper Airborne Observatory (KAO) at an altitude of 41,000 feet using our laser heterodyne spectrometer. The observational procedure and technical details of the 1985 flights have been described by ZBG. For the second series in 1986 September, both the mixer and the intermediate-frequency (IF) amplifier were cooled to 77 K, which reduced the system noise temperature to 10,000 K (SSB). The mixer is a GaAs Schottky-diode in a corner-reflector mount, and the local oscillator (LO) is an optically pumped $^{15}NH_3$ laser. The fixed LO frequency is 802.986 GHz, which is offset 6.3 GHz from the $J = 2$–1 C I line.

A filterbank with 40 5-MHz channels provided a velocity resolution of 1.85 km s^{-1} over an interval of 74 km s^{-1}. For the 1986 flights, a 64 × 20 MHz filterbank was used simultaneously to provide a wide view of the spectrum over 474 km s^{-1} at a resolution of 7.4 km s^{-1}. The chopping secondary of the telescope was switched at 2 Hz with a 7′ throw. The absolute calibration was derived from raster scans of the telescope beam across Jupiter (see § III). These measurements also provided the beam size (80″ FWHM; corrected for the partially resolved Jupiter), the net main beam coupling efficiency ($\eta_{MB} = 0.3$), and the instrument boresight (to 15″). The net coupling efficiency includes losses due to spillover, the central blockage, sidelobes, the pressure-window transmission (80%), and the deviation of the chopper waveform from a square wave. These individual contributions to the measured net coupling efficiency are common to observations of all the sources, and are not separable in the data presented here. Jupiter was assumed to have a uniform elliptical intensity distribution with major and minor axes of 45″ × 48″ for the 1985 flights, and 46″ × 49″ for the 1986 flights. The brightness temperature of Jupiter at 370 μm was taken to be 160 K (Hildebrand *et al.* 1985).

b) *Sources of Systematic Uncertainty*

The largest source of uncertainty for airborne observations is the source coupling, which quantifies how well the astronomical source fills the telescope antenna pattern. The source coupling differs for the $J = 2$–1 and $J = 1$–0 observations, because the telescope beamwidth is 3′ for the 492 GHz observations and 1.′5 for the 809 GHz observations, and the sources are usually comparable in size (3′–10′) to the beams. Furthermore, a calculation of the source coupling efficiency requires knowledge of the entire telescope antenna pattern, including sidelobes, as well the spatial intensity distribution of the astronomical source. This information is generally not available, so educated guesses must be made, as is discussed in § III. The source coupling uncertainty can be removed if both telescope beams are small enough that the source can be reasonably assumed to have a uniform intensity over the beam areas, but this will require larger airborne or space-based telescopes.

Atmospheric transmission is not a source of systematic uncertainty in airborne observations of C I, because the transmission in both sidebands is essentially perfect. This is in contrast to the situation for ground-based observations at both 492 and 809 GHz. Even at the 4.2 km altitude of the best mountain sites such as Mauna Kea, the transmission at these frequencies is usually less than 30%, and variability on the time scale of hours can be large. Consequently, calibration is more difficult than it is in airborne work. The 492 GHz C I observations of Phillips and Huggins (1981) with which we compare our 809 GHz data were performed on the KAO and likewise do not suffer from atmospheric transmission uncertainties.

c) *Results*

Figures 1*a* through 1*d* show our results on the C I $^3P_2$–$^3P_1$ line from observations of OMC 1, NGC 2024, W3, and S140 done in 1986 September. For comparison, spectra of the corresponding 1–0 line at 492 GHz taken from Phillips and Huggins (1981) are also plotted. Three positions in DR21 were also observed, and the results are shown in Figure 2, along with a map of the $^{12}C^{16}O$(1–0) integrated intensity labeled with the observed positions. No baseline corrections or smoothing were applied to the 1986 data. Whenever possible, the positions observed were chosen to match those of the 1–0 observations. Our 1985 July results on the 2–1 line in W51, M17, W3, and DR21 are shown in ZBG. The C I line centers, widths (FWHM), peak temperatures and their uncertainties are listed in Table 1 for both transitions. In most cases, these parameters were deduced from Gaussian fits to the data for both transitions. For W3 and DR 21(OH) (position 1 in Fig. 2), we list the 1986 results only since these data are of higher quality, although the 1985 data are consistent within the uncertainties. The velocity scale for the [C I] 1–0 data presented by Phillips and Huggins (1981) was based on a transition frequency of 492.1623 GHz, as measured by Saykally and Evenson (1980). Since then, this frequency has been revised to 492.1612 GHz by Cooksy *et al.* (1986), which corresponds to a velocity shift of 0.7 km s^{-1}. A discrepancy between CO and [C I] velocities in astronomical sources of about this magnitude was also noticed by Phillips *et al.* (1980). Therefore, we have shifted the spectra of Phillips and Huggins (1981) by −0.7 km s^{-1}. This shift is incorporated in the line parameters presented in Table 1 as well as in the spectra plotted in Figures 1 and 2. Data taken from Keene *et al.* (1985) were not shifted because they already incorporate a velocity correction. In most cases, the line centers and widths agree reasonably well. The substantially different line widths for W3 may be due to beamsize effects since CO maps show that W3 has a complex velocity structure (Brackmann and Scoville 1980).

The accuracy of the Doppler velocity scale for our $J = 2$–1 data depends on both the laboratory measurement of the C I line and our knowledge of the laser LO frequency. The statistical accuracy of the $^3P_2$–$^3P_1$ rest frequency measurement is 1 MHz at the 99.95% (3.5 σ) confidence limit (A. Cooksy 1988, private communication), and the systematic uncertainty is 0.3 MHz at the same confidence level (K. Evenson 1988, private communication). Our laboratory measurement of the $^{15}NH_3$ laser frequency is 802.9860 ± 0.0005 GHz. Were the laser to be mistuned, its output frequency could differ by as much as 2 or 3 MHz from the value quoted above. We are careful, however, to

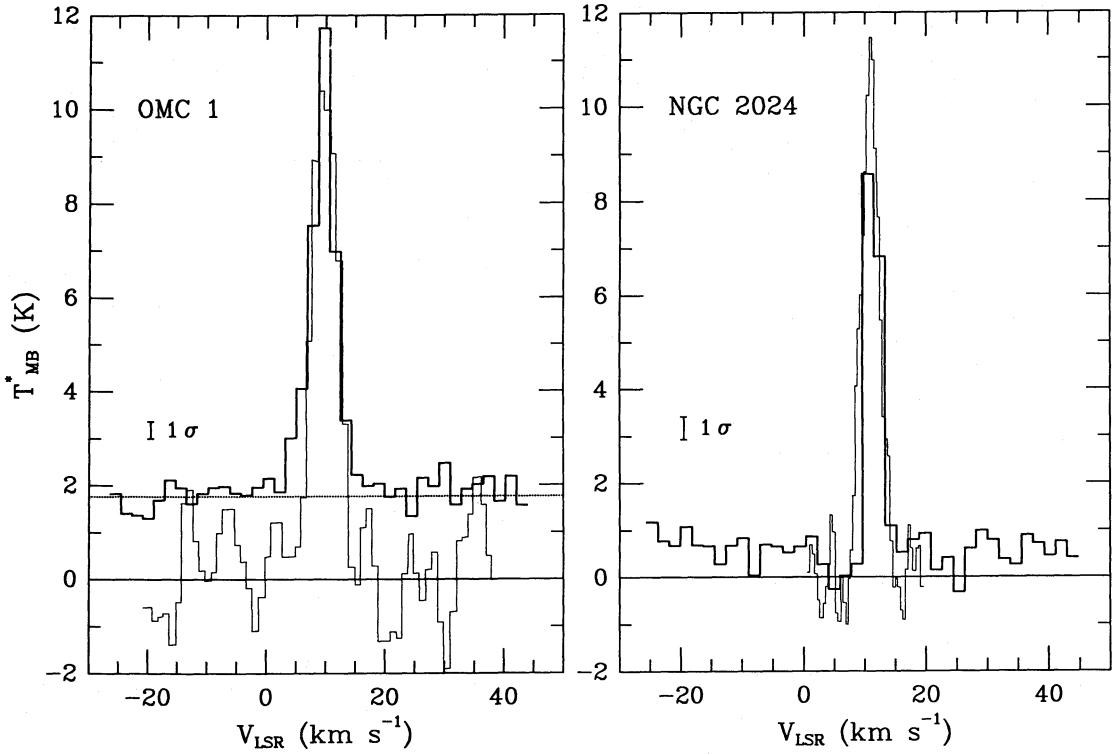

FIG. 1a

FIG. 1b

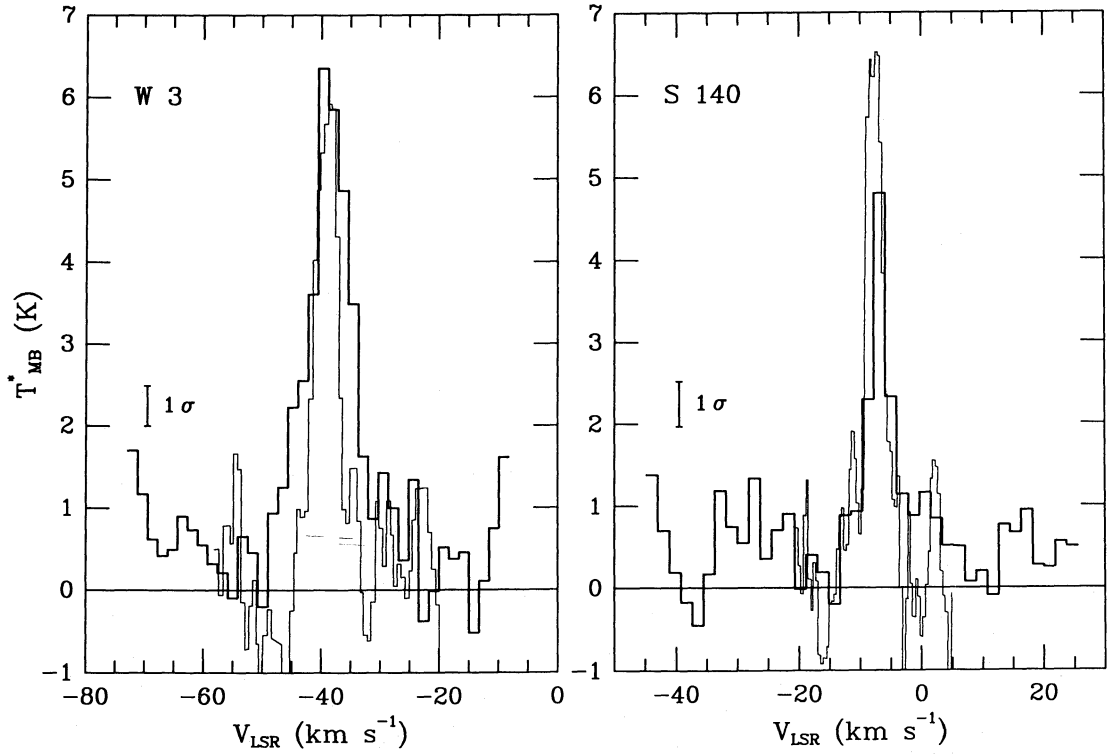

FIG. 1c

FIG. 1d

FIG. 1.—809 GHz [C I] $^3P_2$–$^3P_1$ emission (*heavy line*) observed toward (*a*) OMC 1, integration time of 60 minutes; (*b*) NGC 2024, integration time of 32 minutes; (*c*) W3, integration time of 32 minutes; and (*d*) S140, integration time of 26 minutes. The $^3P_1$–$^3P_0$ data (*light line*) of Phillips and Huggins (1981) are also shown. The 2–1 data were obtained in 1986 September. The dotted line in (*a*) shows the expected 370 μm continuum emission in a 90″ beam (Keene, Hildebrand, and Whitcomb 1982) corrected for the dewar window transmission in each sideband. Statistical uncertainties of 1 σ are shown for the $^3P_2$–$^3P_1$ data only.

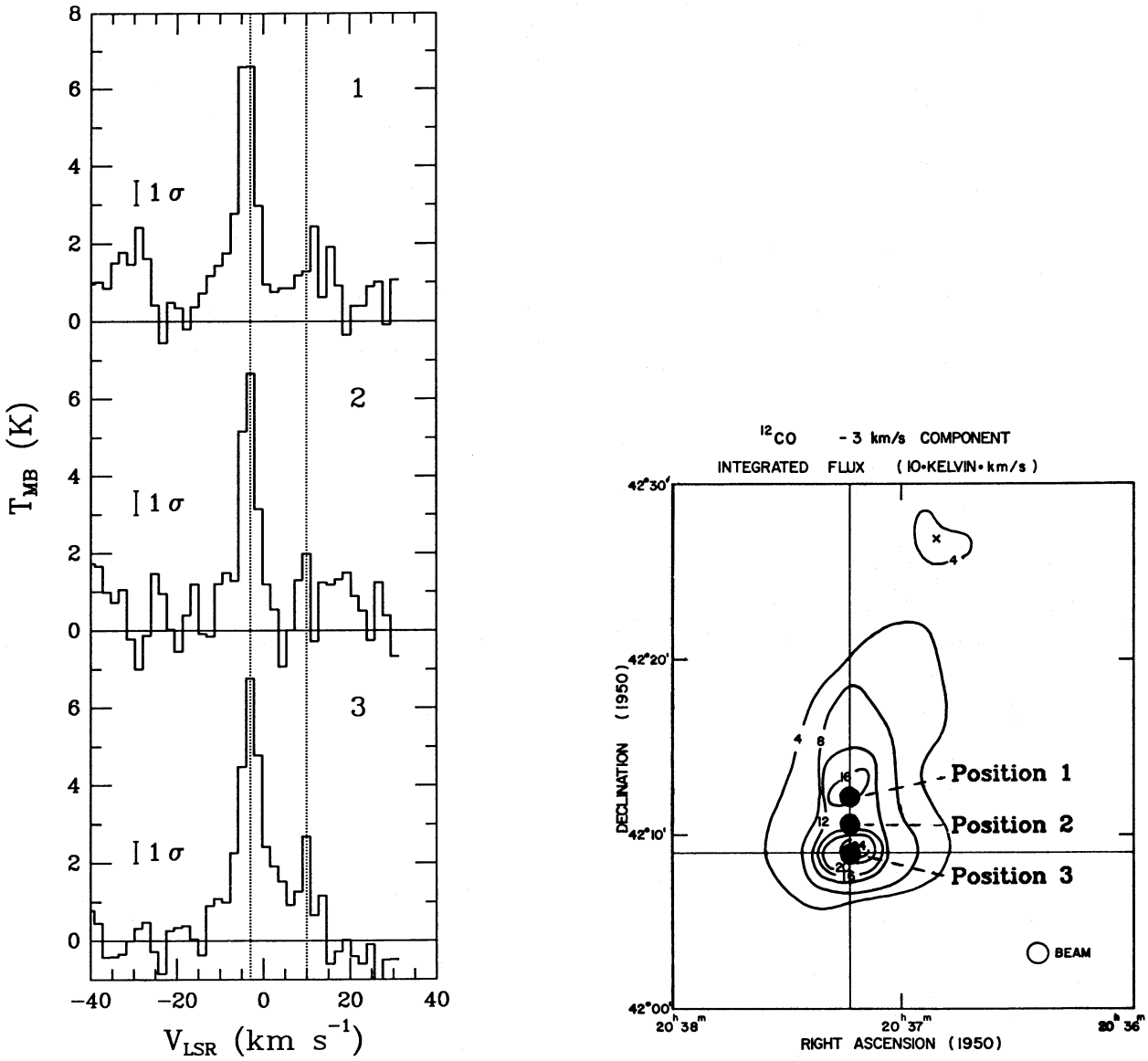

FIG. 2.—809 GHz [C I] $^3P_2$–$^3P_1$ emission observed toward three locations in DR21. Integration times are 20 minutes for position 1 [DR21(OH)] and position 2 and 24 minutes for position 3. Also shown is a map of the CO(1–0) integrated intensity (Dickel, Dickel, and Wilson 1978) labeled at the observed positions with dark circles, which indicate the beam size of the [C I] 2–1 observations. Dotted lines are drawn at −3 and +10 km s^{-1} where microwave emission from CO is observed.

keep the laser cavity tuned to the peak of the power output curve, and consequently our uncertainty is the 0.5 MHz value quoted above. The total 2 σ uncertainty in the frequency accuracy of our C I observations is 1.7 MHz, which corresponds to a conservative velocity scale accuracy of 0.65 km s^{-1}. From the difference between the C I and LO frequencies, we get an IF center frequency of 6.3 GHz.

III. CALIBRATION AND SOURCE COUPLING

If the [C I] emitting region is hot ($kT_x \gg h\nu_{21}$; here T_x is the [C I] excitation temperature), optically thin, and sufficiently dense for the transitions to be thermalized, then the 2–1 line will be twice as bright (in temperature units) as the 1–0 line. If the gas is cool ($T_x \sim 20$ K) and optically thick, the 2–1 line will be about half as bright. Given this limited dynamic range, it is important to consider the effects of systematic calibration errors (such as source coupling) on the line intensities prior to deriving excitation temperatures and optical depths. For this reason, we will present a detailed discussion of calibration procedures and their implications for source coupling.

In general, we can express the signal power per unit bandwidth incident on the receiver in one polarization from the astronomical source as (Kutner and Ulich 1981):

$$S_r = \eta_c \, kT_R \frac{\int d\Omega P_n(\Omega) B(\Omega)}{\Omega_A} , \quad (1)$$

where $P_n(\Omega)$ is the normalized telescope beam pattern [$P_n(0) = 1$], $B(\Omega)$ is the normalized spatial intensity distribution of the source [$B(0) = 1$], T_R is the peak Rayleigh-Jeans radiation temperature of the source ($I = 2kT_R/\lambda^2$ is the peak specific intensity), η_c is the net telescope coupling efficiency, and Ω_A is the antenna solid angle $\int d\Omega P_n(\Omega)$. The beam pattern $P_n(\Omega)$ is usually axially symmetric and consists of a central main beam

TABLE 1

C I LINE PARAMETERS

Source	$T_{MB}(2-1)$ (K)	$T_A^*(1-0)$ (K)	$V_{LSR}(2-1)$ (km s^{-1})	$V_{LSR}(1-0)$ (km s^{-1})	$\Delta V(2-1)$ (km s^{-1})	$\Delta V(1-0)$ (km s^{-1})
OMC 1	9.7 ± 0.4	11.7 ± 0.7	9.6 ± 0.1	9.9 ± 0.1	4.3 ± 0.2	4.6 ± 0.4
NGC 2024[a]	8.8 ± 0.5	11.1 ± 0.3	11.3 ± 0.1	10.5 ± 0.1	3.4	3.4 ± 0.1
W3	5.5 ± 0.4	6.2 ± 0.4	−38.5 ± 0.3	−39.7 ± 0.1	8.0 ± 0.6	4.3 ± 0.3
S140[b]	4.5 ± 0.5	4.1	−6.8 ± 0.2	−7.2	3.3 ± 0.4	2.6
W51	8.9 ± 1.0	8.0 ± 0.2	57.5 ± 1.0	58.5 ± 0.3	16.0 ± 2.2	18.8 ± 0.8
M17[b]	12.9 ± 1.3	11.0	19.6 ± 0.7	20.5	6.7 ± 0.8	6.4
DR 21(OH)[c]	6.7 ± 0.7	6.5	−3.9 ± 0.2	...	4.1 ± 0.5	5.0

[a] The 2–1 line width cannot be determined unambiguously since emission was observed in two channels only; hence, the 1–0 width was assumed.

[b] The 1–0 line parameters were taken from Keene *et al.* 1985 and were *not* deduced from the fit, so no uncertainties are listed. This more recent data for the 1–0 line in S140 supercedes the earlier results of Phillips and Huggins shown in Fig. 1. In reference to the Keene *et al.* 1985 observations, the position for S140 corresponds to the one labeled 0.0, while that for M17 is labeled −1.3

[c] 1–0 parameters from J. Keene (1986, private communication).

NOTE.—The quoted uncertainties are ±1 σ. These uncertainties represent receiver noise only; systematic errors in the intensity calibrations and the velocity scales are not included. In most cases, 1–0 line parameters were derived from our fits to the data presented by Phillips and Huggins 1981, taking into account the Hanning smoothing of their spectra. These spectra were shifted by −0.7 km s^{-1} prior to fitting (*see text*).

and concentric sidelobes, and can be calculated if the telescope illumination is known (Goldsmith 1987). These calculations show that for reasonable choices of illumination of the KAO telescope, the main beam solid angle Ω_M is typically 80%–85% of the total, or

$$\frac{\Omega_M}{\Omega_A} = \frac{\int_{\text{main beam}} d\Omega P_n(\Omega)}{\int_{\text{all lobes}} d\Omega P_n(\Omega)} \sim 0.8 \, . \tag{2}$$

Measurements of the Moon (to obtain Ω_A) and Jupiter (to obtain Ω_M) at 492 GHz (J. Keene 1986, private communication) give reasonable agreement with equation (2). At 809 GHz we only have measurements on Jupiter and so cannot calculate the main-beam efficiency independently of our other coupling factors. It should be emphasized that the KAO telescope is of optical quality, so that calculated beam shapes are expected to be accurate.

Calibration involves measuring the signal power received from a source for which both T_R and $B(\Omega)$ are known, and then using the results to estimate T_R for an astronomical source from the signal power received. For example, the 1–0 data are calibrated using the Moon. The intensity distribution of the Moon is fairly constant over the entire telescope beam [$B(\Omega) = 1$], so $S_\nu(\text{Moon}) = \eta_c k T_R(\text{Moon})$. The antenna temperature T_A^* is then defined in terms of known quantities as the ratio of the power received from the astronomical source to the power received from the Moon, multiplied by the radiation temperature of the Moon:

$$T_A^* = \frac{S_\nu}{S_\nu(\text{Moon})} T_R(\text{Moon}) = \frac{\int d\Omega P_n(\Omega) B(\Omega)}{\Omega_A} T_R \equiv \eta_{1-0} T_R \, , \tag{3}$$

where the source coupling efficiency η_{1-0} for the 1–0 observations has been defined as

$$\eta_{1-0} = \frac{\int d\Omega P_{1-0}(\Omega) B(\Omega)}{\Omega_A} \, . \tag{4}$$

If the source is large enough to fill the telescope beam including all sidelobes uniformly, then $\eta_{1-0} = 1$. In the usual case, the source does not fill the beam completely, and $\eta_{1-0} < 1$.

The 2–1 data were calibrated using Jupiter. Since Jupiter is not large enough to fill the main lobe of the telescope beam, the telescope beam must be mapped on Jupiter to deduce the signal that would have been measured on a source large enough to fill the main lobe. Measuring sidelobe patterns with this technique is not feasible given the signal-to-noise ratio and the limited flight time. The beam was mapped on a 7 × 6 grid with a spacing of 20″ and an integration time of 15 s per point. The data are corrected using an optimal filtering technique for the finite settling time of the lock-in amplifier which measures the signal and are then fitted to a two-dimensional Gaussian profile whose center, amplitude S_0, major and minor $1/e$ widths w_1 and w_2, and orientation of the principal axes are free parameters. The statistical uncertainty in these parameters is less than a few percent and is a negligible source of error in the calibration procedure. The results indicate that the beam is asymmetric, with one width ~20% less than the other. Since the direction of the chop coincides almost exactly with the direction in which the beam is broadened, "ringing" of the chopping secondary is most likely the source of this asymmetry. The beam asymmetry does not affect the calibration since the total power in the beam is unchanged. It does, however, affect the source coupling to some degree, but is not likely to be important since the sources are at least a factor of 2 larger than our beam.

The main lobe solid angle is determined from the measured scan using

$$\eta_c k \frac{\Omega_M}{\Omega_A} = \frac{S_0 w_1 w_2}{T_R(\text{Jup}) ab} \, , \tag{5}$$

where a and b are the major and minor semidiameters of Jupiter (Zmuidzinas 1987). T_R(Jup) is calculated to be 141 K by assuming that Jupiter radiates like a 160 K blackbody at 370 μm (Hildebrand *et al.* 1985).

Calibration of the $J = 2$–1 main beam line intensities consists of dividing the power received (eq. [1]) by $\eta_c k \Omega_M / \Omega_A$ (eq. [5]):

$$T_{MB} = T_R \frac{\int d\Omega P_{2-1}(\Omega) B(\Omega)}{\Omega_M} \equiv \eta_{2-1} T_R \, . \tag{6}$$

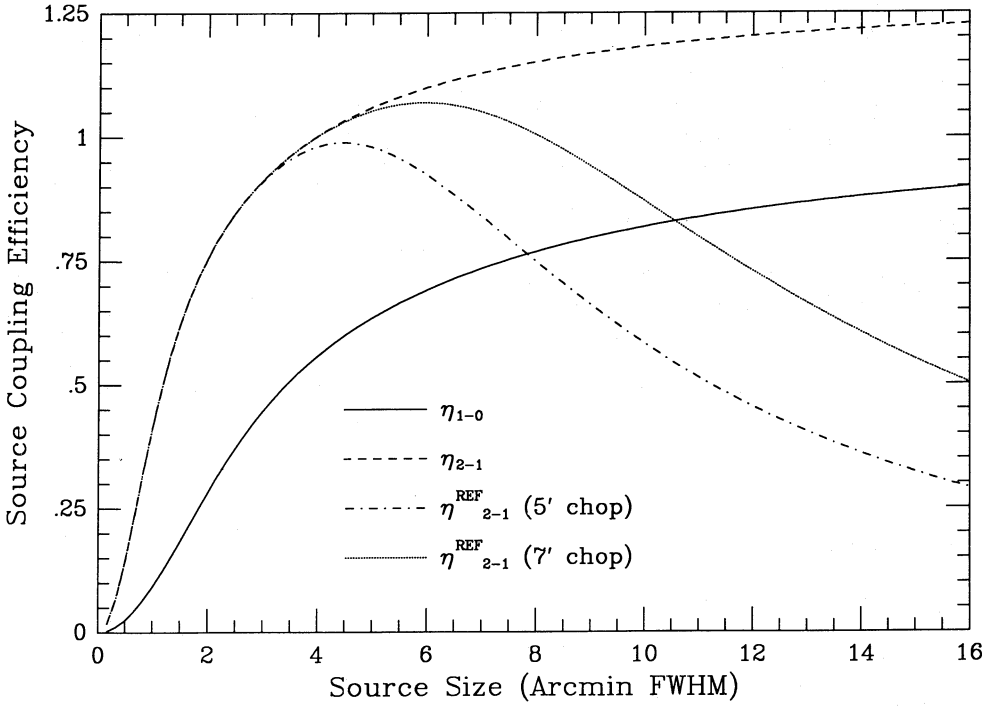

FIG. 3.—*Solid line:* source coupling efficiency η_{1-0} for the 1–0 observations as a function of source size. *Dashed line:* source coupling efficiency η_{2-1} for the 2–1 observations. *Dot-dashed line:* η_{2-1} corrected for emission in the reference beam for a 5′ chopper throw. *Dotted line:* η_{2-1} corrected for a 7′ throw.

The last equality defines the source coupling efficiency for the 2–1 observations, η_{2-1}. For a source which completely fills the main beam uniformly but does not fill any sidelobes $\eta_{2-1} = 1$. For a source which fills the main beam as well as some sidelobes, $\eta_{2-1} > 1$, since only the power in the main beam is used in the calibration. Both η_{1-0} and η_{2-1} were calculated using theoretical telescope beam patterns and sources with a Gaussian intensity distribution. The results are plotted in Figure 3 as a function of source size. As can be seen in this figure, the chosen illumination produces a main beam containing 80% of the total radiated power ($\eta_{2-1} \rightarrow 1.25$ for large sources). For large source sizes, emission in the reference beams of the 2–1 observations must also be considered, since this emission reduces the apparent line intensity. Therefore, we calculate η_{2-1} corrected for emission in the reference beams (again assuming a Gaussian intensity distribution) and plot the results in Figure 3 for the 5′ and 7′ chopper throws used in the 1985 and 1986 observations, respectively.

IV. MODEL CALCULATIONS: UNIFORM EMISSION REGION

a) *Density Required for Thermal Equilibrium*

The A-coefficients and collisional de-excitation rates ($\gamma_{ji} = \langle \sigma_{ji} v \rangle$ for collisions with H atoms) for the ^3P transitions of C I are listed in Table 2, along with the critical densities (the densities for which collisional and radiative rates are equal: $n_{cr} = A_{ji}/\gamma_{ji}$). The line intensities produced from a uniform emission region in which the levels are populated according to thermal equilibrium are easily calculated. These intensities depend only on the temperature and the C I abundance, so a measurement of both line intensities in principle provides sufficient information to determine these parameters. The assumption of equilibrium implies that we are considering regions with densities of $n(H_2) \geq 10^4$ cm^{-3}, larger than the critical density of either transition. Zmuidzinas (1987) discusses this point in more detail, including the suggestion of Monteiro and Flower (1987) that the collision rate of the 1–0 transition could be smaller by more than one order of magnitude as compared to the 2–1 and 2–0 transitions for collisions involving He or H_2. The conclusion is that deviations from thermal equilibrium line intensity ratios only become significant for densities less than 2–3 $\times$ 10^4 cm^{-3}.

Densities greater than 10^4 cm^{-3} are not considered to be large for the regions we observed near the dense cores of molecular clouds. Studies of CS rotational transitions in M17, S140, and NGC 2024 (Snell *et al.* 1984*a*) have shown that average H_2 densities of 5 $\times$ 10^5–10^6 cm^{-3} are common in the cores of molecular clouds. These densities are derived from LVG (large velocity gradient) excitation models and are quite uniform over regions with sizes of 4′–6′. The CS column densities, on the other hand, are smaller by one order of magnitude at the edges than at the centers of the regions observed. This suggests that the clouds consist of high-density clumps interspersed with lower density gas, and that the beam filling factor of these clumps varies from $\sim$1 near the centers to $\sim$0.1 at the edges, for the 1′ beam used in these observations. Similar multi-

TABLE 2

C I TRANSITION DATA

LEVEL		A_{ji}	$\gamma_{ji} = aT^b$ cm^3 s^{-1}		$n_{cr}(T = 50$ K)
j	i	(s^{-1})	a	b	(cm^{-3})
$^3P_1$	$^3P_0$	7.93 $\times$ 10^{-8}	1.3 $\times$ 10^{-10}	0.045	5.1 $\times$ 10^2
$^3P_2$	$^3P_1$	2.68 $\times$ 10^{-7}	7.8 $\times$ 10^{-11}	0.035	3.0 $\times$ 10^3
$^3P_2$	$^3P_0$	2.0 $\times$ 10^{-14}	2.0 $\times$ 10^{-10}	0.084	...

NOTE.—A-coefficients are from Nussbaumer 1971. The collisional rates are due to Launay and Roueff 1977, as parameterized by Tielens and Hollenbach 1985*a*.

transition studies of H_2CO (Mundy *et al.* 1987) indicate the presence of an additional component of gas with a density of $\geq 10^4$ cm^{-3}, which is likely to be foreground or interclump gas. These conclusions are supported by submillimeter dust continuum measurements, which indicate average core densities of $\geq 10^5$ cm^{-3} (OMC 1: Keene, Hildebrand, and Whitcomb 1982; W3: Jaffe *et al.* 1983; W51: Jaffe, Becklin, and Hildebrand 1984; see also Schloerb, Snell, and Schwartz 1987).

Large densities are also likely if the [C I] emission arises in photodissociation regions, given the strong [O I] 63 μm and 145 μm lines observed in the photodissociation regions of several clouds (Crawford *et al.* 1986; Genzel and Stacey 1985). The large critical densities of these lines ($>10^5$ cm^{-3}) combined with their large intensities indicate hydrogen densities of $\sim 10^5$ cm^{-3} for these regions (Stacey 1985), provided that the optical depths are not too large.

b) Methodology

The line radiation temperature emitted by a region of uniform excitation temperature is given by the usual formula:

$$T_R(j-i) = \frac{h\nu/k}{e^{h\nu/kT_x} - 1}\,(1 - e^{-\tau_{ji}})\,. \tag{7}$$

Under the assumption that the levels are thermally populated with an excitation temperature T_x, the ratio of the 1–0 and 2–1 optical depths is given by

$$\rho(T_x) = \frac{\tau_{21}}{\tau_{10}} = 1.28 \exp\left(\frac{-23.6}{T_x}\right) \frac{1 - \exp(-38.8/T_x)}{1 - \exp(-23.6/T_x)}\,. \tag{8}$$

This ratio is plotted in Figure 4. From this figure, we can see that $\tau_{21} \leq \tau_{10}$ for $T_x \leq 50$ K, while $\tau_{21} \geq \tau_{10}$ for $T_x \geq 50$ K. This ratio approaches the limiting value of 2.1 for large temperatures. Thus, given T_x and τ_{10}, we can calculate τ_{21} from equation (8) and both line intensities from equation (7). In most cases, this procedure is invertible. That is, if we are given the intensities $T_R(1\text{–}0)$ and $T_R(2\text{–}1)$ at the line center velocity V_0, we can find the corresponding values of T_x and τ_{10}. However, there are cases for which two solutions (T_x, τ_{10}) exist, as well as cases for which no solutions exist. These situations as well as the effects of finite measurement uncertainties are discussed in depth by Zmuidzinas (1987). If T_x and τ_{10} are known, the column density can be calculated from

$$N_{CI} = 0.47\tau_{10}(V_0)\,\Delta V\,\frac{f(T_x)}{1 - \exp(-23.6/kT_x)}\,, \tag{9}$$

where N_{CI} is in units of 10^{17} cm^{-2} and ΔV is the equivalent width of the velocity distribution in km s^{-1}. For a Gaussian profile, the equivalent width ΔV is given in terms of the full width to half-maximum ΔV_{FWHM} by $\Delta V = [\pi/(4 \ln 2)]^{1/2}\,\Delta V_{FWHM} = 1.06\,\Delta V_{FWHM}$. We will generally ignore the distinction between ΔV and ΔV_{FWHM}. Also, we do not perform opacity corrections on the measured line widths, since such corrections are generally small.

V. EXCITATION TEMPERATURES AND OPTICAL DEPTHS

As in ZBG, we derive T_x and τ_{10} for three sets of line intensities. The first set (A) is given by $T_R(1\text{–}0) = T_A^*(1\text{–}0)$ and $T_R(2\text{–}1) = T_{MB}(2\text{–}1)$. For this oversimplified case, we use the line intensities exactly as they are given in Table 1 and perform no corrections for beam filling effects. The resulting values of T_x and τ_{10} are listed in Table 3, along with 95% confidence lower limits for T_x and upper limits for τ_{10}. These limits are based on the statistical uncertainties of the line intensities as listed in Table 1. The method with which these confidence limits were derived is discussed by Zmuidzinas (1987). In cases for which

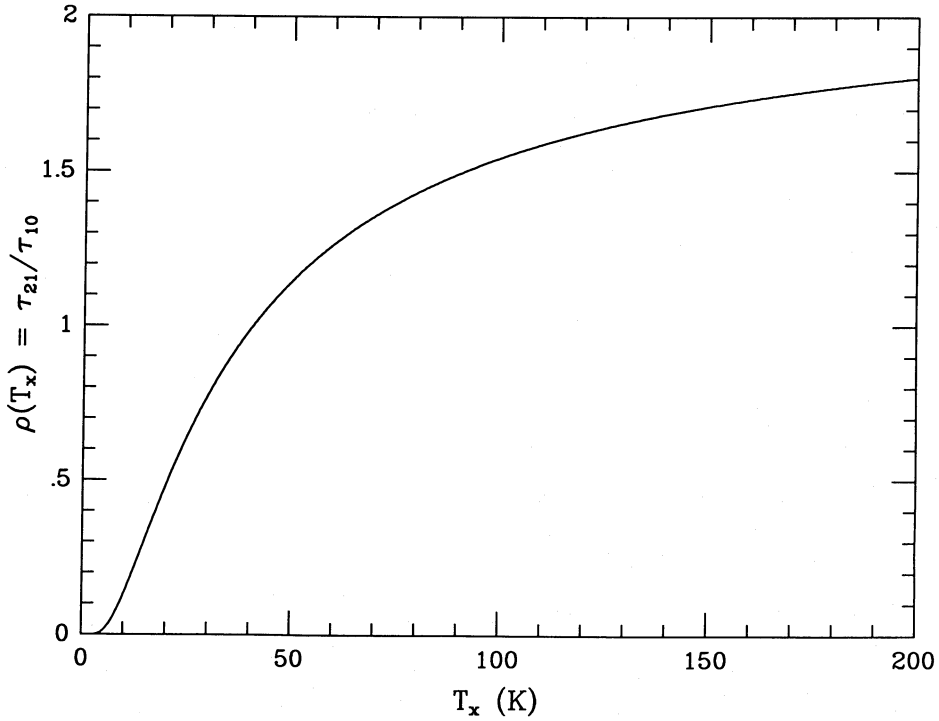

FIG. 4.—Ratio of [C I] optical depths as a function of excitation temperature

TABLE 3

OPTICAL DEPTHS AND EXCITATION TEMPERATURES

Source	(A) UNCORRECTED[a]				(B) CORRECTED[b]				(C) CORRECTED[c]				
	T_x	T_{LL}[d]	τ_{10}	τ_{UL}[e]	T_x	T_{LL}[d]	τ_{10}	τ_{UL}[e]	T_x	T_{LL}[d]	τ_{10}	τ_{UL}[e]	θ_S[f]
OMC 1	42.	36.	0.47	0.69	27.	22.	1.6	>2	77.	62.	0.23	0.33	14.
NGC 2024	40.	35.	0.48	0.63	25.	22.	1.3	>2	71.	59.	0.24	0.32	~14
W3	45.	38.	0.11	0.16	25.	21.	1.25	>2	25.	21.	1.25	>2	3.5
S140	61.	42.	0.09	0.17	...	...	...	...	...	...	...	...	...
W51	64.	47.	0.17	0.25	37.	21.	0.51	0.81	64.	46.	0.22	0.37	7.8
M17	72.	53.	0.20	0.31	36.	26.	0.95	>2	48.	36.	0.56	0.91	6.2
DR 21(OH)	56.	40.	0.16	0.29	29.	19.	0.60	1.7	32.	19.	0.55	1.4	6.

[a] Derived from measured line intensities with no correction for source coupling effects.
[b] Corrected for source coupling only using a source size of θ_S.
[c] Corrected for source coupling and reference beam emission using a source size of θ_S.
[d] Lower limit for T_x (95% confidence level).
[e] Upper limit for τ_{10} (95% confidence level).
[f] θ_S is either the [C I] or ^{12}CO(1–0) source size (FWHM arcmin). The sizes are from Phillips and Huggins 1981 ([C I] in OMC 1); Kutner *et al.* 1977 (CO in NGC 2024); Brackman and Scoville 1980 (CO in W3); Mufson and Liszt 1979 (CO in W51); Keene *et al.* 1985 ([C I] in M17); and Dickel, Dickel, and Wilson 1978 (CO in DR 21).

the 1–0 uncertainty was not available, the 2–1 and 1–0 intensities were assumed to have equal uncertainty.

The second set (B) is given by $T_R(1\text{–}0) = T_A^*(1\text{–}0)/\eta_{1-0}$ and $T_R(2\text{–}1) = T_{MB}(2\text{–}1)/\eta_{2-1}$. The resulting values of T_x and τ_{10}, as well as the source sizes used in estimating the source coupling coefficients, are listed in Table 3 (see also Fig. 3) and are derived from maps of $J = 1\text{–}0$ ^{12}CO emission, except in cases for which the [C I] source size is known (OMC1; M17). Scans of the [C I] 1–0 emission in OMC 1 (Phillips and Huggins 1981) and M17 and S140 (Keene *et al.* 1985) indicate that the C I emission region is similar in extent to the CO emission region. Furthermore, the [C I] 2–1 emission is also likely to have a similar spatial distribution judging from the constant intensities measured at three positions separated by 4′ in DR 21. Additional evidence for extended 2–1 emission is provided by our observations of S140. Keene *et al.* (1985) have shown the 1–0 emission to be extended over more than 10′ in S140. Our data indicate that the 2–1 emission in S140 is also spread over at least 7′ in the NE–SW direction of the Keene *et al.* scan, because chopping in the direction of the scan fails to show any differential emission in the $J = 2\text{–}1$ line, while chopping perpendicular to this direction yields the line shown in Figure 1. Unfortunately, the position we observed in S140 was quite near the ionization front, and it is difficult to estimate a reliable source coupling efficiency for this position given the size and pointing uncertainty of the 1–0 beam; thus, S140 is not listed in Table 3.

The third set of intensities (C) for which we calculated T_x and τ_{10} is the same as the second set (B) but with η_{2-1} replaced by η_{2-1}^{REF}. This extra correction accounts for possible emission in the "off-source" reference beam because of the large source size. The results are listed in Table 3.

As can be seen from Table 3, the derived excitation temperatures and optical depths are sensitive to the source correction applied, especially to the large upward corrections of the 1–0 intensity. In contrast, the statistical uncertainties are in most cases negligible. For case C, which is probably the most realistic given the evidence for extended 2–1 emission, the results show that $\tau_{10} < 1$ in most cases, and that the excitation temperatures are typically 30–80 K. However, the sensitivity of the results to the source coupling corrections precludes putting strict limits on the optical depths and excitation temperatures.

VI. COMPARISON WITH CO ABUNDANCE

Since our evidence points to optically thin [C I] lines, the lower limits to the C I column densities derived by Phillips and Huggins (1981) using an optically thin approximation with $T_x = 20$ K are likely to be the actual column densities. The column densities derived in this approximation depend mainly on the measured line integrated intensity and are very insensitive to the assumed excitation temperature, varying by only 25% over the range $15\text{ K} \leq T_x \leq 200$ K. Thus, the column density estimates can be expected to be valid even if variations in the excitation temperature exist along the line of sight or within the beam, as long as the line is optically thin. On the other hand, the CO column density estimates are more uncertain. The standard method for estimating the CO column density involves measuring the intensity of the optically thick ^{12}CO(1–0) line to deduce the excitation temperature, and using this temperature in conjunction with the intensity of an optically thin isotopic line such as ^{13}CO(1–0) or $^{12}C^{18}O$(1–0) to derive the column density of the isotopic species, which is then used along with an assumed relative abundance to calculate the ^{12}CO column density. The sensitivity of the result to the assumption that the optically thick ^{12}CO line measures the average excitation temperature within the cloud is easily demonstrated. The intensity of the isotopic CO line essentially measures the column density of CO in the $J = 1$ state. The fraction of CO in the $J = 1$ state is inversely proportional to the partition function $f(T_x)$ and consequently the total derived CO column density is proportional to $f(T_x)$. Since $f(T_x) \propto T_x$ in the classical limit, the derived column densities are directly proportional to the assumed excitation temperatures. In this case, line of sight variations in the excitation temperature will lead to errors, particularly when the temperature of the foreground gas preferentially sampled by the optically thick ^{12}CO line is not representative of the average temperature throughout the cloud. Other sources of error are the possible non–LTE level populations for high-J states and the uncertainties in the relative abundances of the isotopic species of CO.

With these warnings in mind, we present a comparison of CO and C I abundances in Table 4. The CO column density estimates generally agree with those presented by Phillips and Huggins (1981) although in most cases they were derived from

TABLE 4

COMPARISON OF C I AND CO ABUNDANCES

Source	T_x(C I) (K)	T_x(CO) (K)	T_{dust} (K)	N_{CI} (10^{17} cm^{-2})	N_{CO} (10^{18} cm^{-2})	N_{CI}/N_{CO}
OMC 1	77.	70.	70.	9.5	21.	0.05
NGC 2024	71.	38.	40.	7.0	15.	0.05
W3	25.	36.	50.	10.6	11.	0.10
W51	64.	30.	45.	31.0	21.	0.15
M17	48.	35.	50.	18.0	23.	0.08
DR 21(OH)	32.	27.	40.	6.3	12.	0.05

NOTE.—The CO column densities and excitation temperatures were taken from or derived from data in: Schloerb *et al.* 1987 (OMC 1, W51); Phillips and Huggins 1981 (NGC 2024); Loren *et al.* 1981 (NGC 2024); D. T. Jaffe 1987, private communication (W3, W51, DR 21); Thronson and Lada 1983 (M17); Dickel, Dickel, and Wilson 1978 (DR 21). The dust temperatures were taken from Werner *et al.* 1976 (OMC 1); Thronson *et al.* 1984 (NGC 2024); Werner *et al.* 1980 (W3); Harvey *et al.* 1986 (W51, DR 21); and Gatley *et al.* 1979 (M17).

independent data. The column densities of C I are derived from the case C optical depths and excitation temperatures listed in Table 3. It is important to remember that these are peak column densities since they were derived from intensities corrected for source coupling; beam-averaged column densities would be smaller. The C I (Table 3) and CO excitation temperatures as well as dust temperatures are also listed in Table 4 for comparison. The CO temperatures were not corrected for possible self-absorption, although there is some evidence that doing so results in temperatures which more closely match those measured from the thermal dust emission (Phillips *et al.* 1981).

VII. EFFECTS OF SUBCRITICAL DENSITIES

While there seems to be no doubt that significant amounts of high-density gas are present in the clouds we have observed, what is not certain is whether the [C I] emission arises in these high-density regions or in the lower density gas which envelops the dense cores. It is therefore important to examine the effects of subcritical densities on our conclusions, which are derived on the basis of thermal equilibrium. Obviously, a unique solution for all three parameters (i.e., kinetic temperature, H_2 density, and C I column density) is not possible with just two [C I] line intensities, so additional assumptions are needed. We proceed by assuming that the brightness temperature of the (optically thick) ^{12}CO line measures the kinetic temperature of the [C I] emission region. The two [C I] lines may then be used to deduce or constrain the two remaining parameters: $n(H_2)$ and N_{CI}. Our C I excitation models incorporating the escape probability approximation in a plane-parallel region (Scoville and Solomon 1974) show that if $T_{kin} \geq 30$ K, $T_A^*(1\text{–}0) \leq 12$ K, and $T_{MB}(2\text{–}1)/T_A^*(1\text{–}0) \geq 0.5$, then $\tau_{10} < 1$. Tables 1 and 4 show that these inequalities are satisfied by all of the sources observed, so the [C I] lines are optically thin in this model as well. If the [C I] lines are optically thin, then the observed ratio of the 2–1 and 1–0 intensities may be used to constrain the density of the [C I] emission region. For instance, if the radiation temperatures of the two lines are equal, the density must be larger than $\sim 10^3$ cm^{-3}. Also, the excitation calculations indicate that the intensity of the 1–0 line still measures essentially only the C I column density if the H_2 density is ≥ 500 cm^{-3}, for kinetic temperatures of 30 K or larger, since such temperatures and densities result in 1–0 excitation temperatures of at least 15 K (see § VI). We conclude that the column density estimates are not likely to be affected by subcritical densities. Densities lower than 10^4 cm^{-3} will mainly cause the kinetic temperature and the C I excitation temperature to differ. [C I] emission region densities lower than $\sim 10^3$ cm^{-3} are excluded by the data.

VIII. LINE WIDTH ARGUMENTS

To date, the only evidence offered in support of large [C I] optical depths is the line width comparison of Phillips and Huggins (1981). In this comparison, an empirical relationship between opacity and line width is established with observations of the 1–0 and 2–1 transitions of the various isotopic forms of CO. The optical depth of the [C I] 1–0 line is then deduced from its line width. The deduced values are $\tau_{10} \sim 25$ for OMC 1 and $\tau_{10} \sim 4$ for NGC 2024, which are based on line widths of $\Delta V = 5.0$ km s^{-1} for OMC 1 and $\Delta V = 4.0$ km s^{-1} for NGC 2024. For comparison, the [^{12}CO(1–0), ^{13}CO(1–0)] line widths listed by Phillips and Huggins for these sources are [5.9, 3.9] km s^{-1} for OMC 1 and [5.1, 3.0] km s^{-1} for NGC 2024. The line widths that we deduce from least-squares fits to the [C I] data in Phillips and Huggins are generally smaller than the values listed in their tables. In our fitting program, the model profile is first degraded by the spectrometer resolution and is then Hanning smoothed, since the $J = 1\text{–}0$ [C I] data are also smoothed. Our fits indicate that the finite resolution and smoothing result in a significant broadening of the line profile, which should be considered prior to a comparison of line widths. The line widths deduced from our fits to the Phillips and Huggins 1–0 [C I] data (see Table 1) are 4.6 ± 0.4 km s^{-1} for OMC 1 and 3.4 ± 0.1 km s^{-1} for NGC 2024, which are consistent with those of our 2–1 line profiles. The optical depths deduced from the corrected line widths, if we follow the original arguments of Phillips and Huggins, are $\tau_{10} \sim 5$ for OMC 1 and $\tau_{10} \sim 0.8$ for NGC 2024. For these lower optical depths, the ratio of column densities N_{CI}/N_{CO} in these two clouds is reduced from ~ 0.7 to ~ 0.14. Moreover, this ratio is subject to the uncertainties in the CO abundance estimates, the uncertainties in the construction of the line width versus opacity relationship, and the strength of the argument that line-width variations are principally due to optical depth effects. Thus, at this point, there seems to be little evidence in favor of optically thick ($\tau \gg 1$) [C I] lines, while evidence to the contrary is provided by the fact that the Planck-corrected [C I] brightness temperatures are substantially smaller than temperatures measured from optically thick ^{12}CO lines or thermal emission from dust. It may be that the [C I] lines become optically thick in more localized regions within specific

clouds, but such a conclusion cannot be deduced from the data currently available with beam sizes greater than 90″.

IX. AN UPPER LIMIT TO HIGH-VELOCITY C I IN OMC 1

a) Review

Extended high-velocity (± 100 km s^{-1}) wings on numerous molecular lines, particularly CO, are observed toward the BN/KL region of OMC 1. Maps of the high-velocity wings of the CO emission (Masson *et al.* 1987; Erickson *et al.* 1982) indicate a bipolar outflow from a central source, perhaps IRc2, extending over a region $\sim 30''$ in diameter. The "hot core" is a 10″ region near the center of the outflow (Morris, Palmer, and Zuckerman 1980), and consists of hot (≥ 150 K), dense ($> 10^6$ cm^{-3}) gas with a relatively low velocity dispersion (10 km s^{-1}). Lobes of H_2 vibrational emission are observed at about $\pm 20''$ along the direction of the outflow from the center and are thought to arise from shocked gas at the interface between the high-velocity (± 100 km s^{-1}) flow and the ambient gas. Velocity-resolved observations of far-infrared CO, OH, and [O I] emission (Crawford *et al.* 1986) arising in the shocked or postshock gas show that these line profiles have widths of 30–50 km s^{-1}, consistent with the H_2 profiles (Nadeau, Geballe, and Neugebauer 1982).

A search for high-velocity [C I] 492 GHz emission was reported by Beichman *et al.* (1982). The primary motivation for this search was to study the effects of shocks or elevated temperatures and densities on the chemistry of CO and C I. For example, Williams and Hartquist (1984) have suggested that shocks may be responsible for the large abundances of C I in molecular clouds. They propose that in dense clouds, mantles are accreted onto dust grains from the gas, and that these mantles are removed by periodically recurring shock waves. If a significant fraction of the mantle material is returned to gas phase in atomic form, and if shocks occur every 10^6 yr, then large C I abundances (C I/CO ~ 0.1) can be maintained. The negative result of Beichman *et al.* in the 1–0 [C I] line has been interpreted as evidence that shocks do not enhance the C I abundance, or that any C I produced in shocks is rapidly converted to CO in the hot, dense postshock gas (e.g., by reactions with H_2). Our high signal-to-noise spectrum (Fig. 5) of the [C I] 2–1 line in OMC 1 allows us to place improved limits on the high-velocity C I abundance. There are two advantages to observing at the higher frequency: (1) for hot gas, the 2–1 line is twice as bright as the 1–0 line; and (2) the beamsize on a given telescope is narrower, so beam dilution is less important.

b) Emission Regions

As already discussed, there are several components in the broad-line emission from BN/KL: the hot core, the outflow, and the shock/postshock region. In general, the relative contribution from each component to the total emission will depend heavily upon the line observed. For example, millimeter-wave CO lines are not very sensitive to the shocked component since the large (750 K) excitation temperature implies that only a small fraction of CO is in low-J states. Conversely, far-infrared CO ($J > 20$) emission does not arise in the hot-core or outflow regions since the excitation is inadequate. C I emission would not necessarily be restricted to any one of these three regions, since each has sufficient excitation to populate substantially all three C I levels. Rather, the emission from a given region depends primarily on the product of C I column density and the beam filling factor of the region, unless the line is optically thick, in which case it depends on the temperature and the filling factor.

c) Hot Core

The mass of the hot core has been estimated to be 9 $M_\odot$ based on interferometric maps of the ^{13}CO(1–0) emission (Masson *et al.* 1987). Working backwards, we deduce that the average ^{12}CO column density in the hot core is $N_{CO} = 1.3 \times 10^{20}$ cm^{-2} based on their assumed relative CO abundance of $[CO]/[H_2] = 1.3 \times 10^{-4}$ and a linear size of 7×10^{16} cm (10″). In turn, this allows an estimate of the [C I] 2–1 optical depth:

$$\tau_{21} \sim 10(N_{C\,I}/N_{CO}) \tag{10}$$

based on an assumed excitation temperature of 150 K and a velocity width of 10 km s^{-1} (FWHM; Genzel *et al.* 1982). Typically, $N_{C\,I}/N_{CO} \sim 0.1$, so $\tau_{21} \sim 1$. From equation (7), we deduce that $T_R(2\text{–}1) \sim 83$ K. The beam dilution factor for a 10″ disk observed by a 90″ FWHM Gaussian beam is $\eta_{2-1} = 8.5 \times 10^{-3}$, so the expected intensity would be $T_{MB} \sim 0.71$ K. Since the noise per 1.85 km s^{-1} channel in the [C I] spectrum shown in Figure 5 is 0.28 K (1 σ), this intensity would have been detectable, especially since it would have covered about five channels. Unfortunately, the presence of the strong emission component from the quiescent molecular cloud overwhelms any such emission over more than half of the expected velocity interval (the hot core is centered at 5.5 km s^{-1}; Genzel *et al.* 1982), making it difficult to set limits on the C I abundance in the hot core. Even so, attempts to fit two Gaussian profiles to the data with the center of one of the components fixed at 5.5 km s^{-1} and its width fixed at 10 km s^{-1} resulted in an amplitude for this component of 0.77 K, while the χ^2 of the fit was reduced by an amount which was almost statistically significant. Thus, a hot core emission component may be present in our data. The emission from the hot core could easily be detected unambiguously with a 3 m airborne telescope if $N_{C\,I}/N_{CO} \sim 0.1$. Higher velocity resolution would also be useful in distinguishing the hot core component from the emission due to the quiescent cloud.

d) The "Plateau" or High-Velocity Flow

The column density of CO in the high-velocity flow can be estimated from the integrated intensity of the CO(2–1) line wings (see Fig. 5). Assuming that the wings are optically thin,

$$I_{ji} = \int T_R(j-i)dV = \frac{hc}{k}\frac{\lambda_{ji}^2}{8\pi} A_{ji} N_j \,. \tag{11}$$

The column densities N_j for C I and CO are related to the total column densities by

$$N_{C\,I}(J=2) = N_{C\,I}\frac{5\exp(-62.4/T_x)}{f_{C\,I}(T_x)} \tag{12}$$

and

$$N_{CO}(J=2) = N_{CO}\frac{5\exp(-16.6/T_x)}{f_{CO}(T_x)} \,. \tag{13}$$

The partition function f_{CO} can be approximated by

$$f_{CO} \sim \frac{2T_x}{5.5\text{ K}} \,. \tag{14}$$

The ratio of C I and CO integrated intensities is given by

$$\frac{I_{CI}}{I_{CO}} = \left[\frac{\lambda_{CI}}{\lambda_{CO}}\right]^2 \frac{A_{CI}}{A_{CO}} \frac{N_{CI}}{N_{CO}} \frac{f_{CO}(T_x)}{f_{CI}(T_x)} \exp\left(\frac{-45.8}{T_x}\right). \quad (15)$$

For $T_x \sim 100$ K (Plambeck, Snell, and Loren 1983; Richardson *et al.* 1985), this gives

$$I_{CI}/I_{CO} = 0.12 N_{CI}/N_{CO}\,. \quad (16)$$

We estimate the CO integrated intensity (see Fig. 5) in the velocity range $V \geq 18.8$ km s^{-1} and $V \leq -0.8$ km s^{-1} to be $I_{CO} = 247$ K km s^{-1}, which corresponds to an average column density of 3×10^{17} cm^{-2} over a 75″ beam. The peak column density is much higher, since the size of the high-velocity flow is $\leq 40''$ (Erickson *et al.* 1982). However, using CO and C I data obtained with similar beam sizes reduces the relative filling factor uncertainty. The omitted velocity interval -0.8 km s$^{-1} \leq V \leq 18.8$ km s^{-1} is estimated to contribute a similar integrated intensity; thus, the column densities we quote are representative of only half of the CO in the flow. If the line wings are optically thick (Plambeck, Snell, and Loren 1983; Richardson *et al.* 1985) with $\tau \sim 3$ then $N_{CO} \sim 10^{18}$ cm^{-2}. These estimates are consistent with others appearing in the literature. For example, Snell *et al.* (1984*b*) give $8.2 M_\odot$ for the total mass in the flow, which gives $\sim 2 \times 10^{18}$ cm^{-2} for the average column density in the 75″ CO beam.

We estimate from our data that the 3 σ upper limit to the [C I] intensity in the same velocity interval (out to the limits of our filterbank) is $I_{CI} \leq 8.14$ K km s^{-1}, which gives a limit on the average column density over a 90″ beam of 8.7×10^{16} cm^{-2}. This estimate was obtained by using the observed CO line wings as a weighting factor to give higher weight to the lower velocity channels which would be expected to have more signal, which results in a minimum uncertainty estimate. Since the C I beam is somewhat larger than the CO beam, we apply a correction factor of 1.4 to the C I column densities and intensities, as is appropriate for a source which is small compared to either beam. Equation (16) gives the limits $N_{CI}/N_{CO} \leq 0.38$ for optically thin CO wings and ≤ 0.12 (3 σ) for optically thick wings. These limits are not restrictive enough to indicate any depletion of C I relative to the quiescent molecular cloud, given the results of §§ VI and VIII.

e) Shocked Gas

From far-infrared observations of CO rotational emission lines, Watson *et al.* (1985) estimate that the CO column density in the shocked gas is 4×10^{17} cm^{-2}, averaged over a 1′ diameter area. After correcting for beam filling (0.27, for a 1′ disk observed by a 90″ FWHM Gaussian beam) and velocity coverage (0.6; based on 30 km s^{-1} FWHM for the line profiles [Crawford *et al.* 1986]), we obtain a limit to the C I column density in this gas of $N_{CI} \leq 5 \times 10^{17}$ cm^{-2}. Thus $N_{CI}/N_{CO} \leq 1.3$ for the shocked gas, which again is not a severe limit.

f) Comparison to the Results of Beichman et. al.

Beichman *et al.* (1982) quote a 3 σ upper limit of 6.9×10^{17} cm^{-2} to the column density of C I in a 40″ diameter disk in the velocity intervals -5 km s$^{-1} \leq V \leq 5$ km s^{-1} and 13 km s$^{-1} \leq V \leq 20$ km s^{-1}. Our limit for the equivalent velocity interval and source size is 3.9×10^{17} cm^{-2}, for $T_x = 100$ K. Thus, we are more sensitive by a factor of 1.8 to high-velocity C I emission, but still have not detected any. Even so, our limit of $N_{CI}/N_{CO} \leq 0.12$ for the case of optically thick line wings is similar to the limit of ≤ 0.13 quoted by Beichman *et al.* This coincidence can be understood as the result of several factors: (1) the limit quoted by Beichman *et al.* is a factor of 4 lower than justified by their data, because their calculation represents

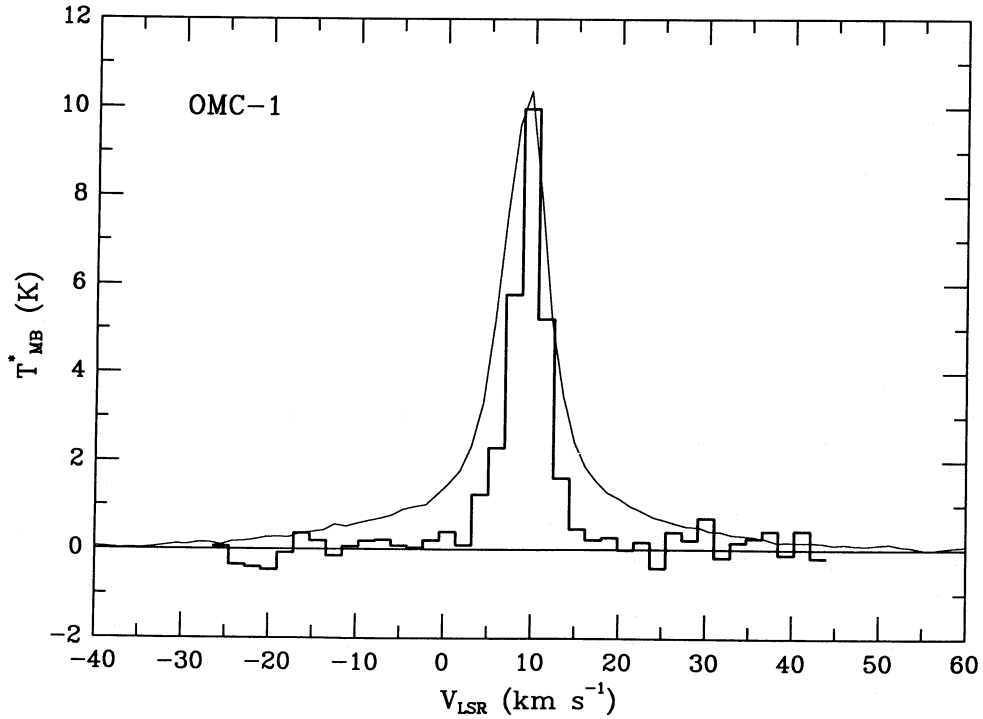

FIG. 5.—$^3P_2$–$^3P_1$ [C I] (*heavy line*) and $^{12}C^{16}O(2–1)$ (*light line*; $\times \frac{1}{8}$) emission toward OMC 1/BN/KL. CO data from Plambeck, Snell, and Loren (1983).

a comparison of the column density of C I in a selected velocity interval with that of CO over the *entire* line profile; (2) our observations have about twice the sensitivity; and (3) our chosen CO column density for the case of optically thick CO line wings is about twice that chosen by Beichman *et al.* The factors of 2 downward (2, 3) cancel the factor of 4 upward (1), resulting in similar numerical values for the abundance ratio.

g) Summary

The ratio of C I to CO in quiescent molecular clouds derived in § VI (see Table 4) is significantly less than that deduced previously, and therefore the upper limit to this ratio in the BN/KL high-velocity flow does not indicate a relative depletion of C I. Thus, models invoking periodic shocks to explain high C I abundances are not contradicted by the existing experimental data. It may be that C I is depleted in these regions; all that we can say is that it is not enhanced substantially. [C I] emission from the hot core may be present in our data but cannot be separated unambiguously from emission produced by the quiescent cloud. Future studies utilizing larger airborne or space-based telescopes will be more sensitive to such emission by at least one order of magnitude.

The staff of the Kuiper Airborne Observatory was very helpful in providing technical assistance during our flight series, and we thank them for their effort. We also thank J. Keene for access to data prior to publication and for valuable discussions. R. T. B. is grateful to the Natural Sciences and Engineering Research Council of Canada for her postdoctoral fellowship. These observations were supported by NASA grant NAG 2-254.

REFERENCES

Beichman, C. A., Phillips, T. G., Wootten, H. A., and Frerking, M. A. 1982, in *Regions of Recent Star Formation*, ed. R. S. Roger and P. E. Dewdney (Dordrecht: Reidel), p. 445.
Brackmann, E., and Scoville, N. 1980, *Ap. J.*, **242**, 112.
Cooksy, A. L., Saykally, R. J., Brown, J. M., and Evenson, K. M. 1986, *Ap. J.*, **309**, 828.
Crawford, M. K., Lugten, J. B., Fitelson, W., Genzel, R., and Melnick, G. 1986, *Ap. J.* (*Letters*), **303**, L57.
Dickel, J. R., Dickel, H. R., and Wilson, W. J. 1978, *Ap. J.*, **223**, 840.
Erickson, N. R., Goldsmith, P. F., Snell, R. L., Berson, R. L., Huguenin, G. R., Ulich, B. L., and Lada, C. J. 1982, *Ap. J.* (*Letters*), **261**, L103.
Gatley, I., Becklin, E. E., Sellgren, K., and Werner, M. W. 1979, *Ap. J.*, **233**, 575.
Genzel, R., Downes, D., Ho, P. T. P., and Bieging, J. 1982, *Ap. J.* (*Letters*), **259**, L103.
Genzel, R., and Stacey, G. J. 1985, *Mitt. Astr. Ges.*, **63**, 215.
Goldsmith, P. F. 1987, *Internat. J. Infrared Millimeter Waves*, **8**, 771.
Graedel, T. E., Langer, W. D., and Frerking, M. A. 1982, *Ap. J. Suppl.*, **48**, 321.
Harvey, P. F., Joy, M., Lester, D. F., and Wilking, B. A. 1986, *Ap. J.*, **300**, 737.
Hildebrand, R. H., Loewenstein, R. F., Harper, D. A., Orton, G. S., Keene, J., and Whitcomb, S. E. 1985, *Icarus*, **64**, 64.
Jaffe, D. T., Becklin, E. E., and Hildebrand, R. H. 1984, *Ap. J.* (*Letters*), **279**, L51.
Jaffe, D. T., Harris, A. I., Silber, M., Genzel, R., and Betz, A. L. 1985, *Ap. J.* (*Letters*), **290**, L59.
Jaffe, D. T., Hildebrand, R. H., Keene, J., and Whitcomb, S. E. 1983, *Ap. J.* (*Letters*), **273**, L89.
Keene, J., Blake, G. A., Phillips, T. G., Huggins, P. J., and Beichman, C. A. 1985, *Ap. J.*, **299**, 967.
Keene, J., Hildebrand, R. H., and Whitcomb, S. 1982, *Ap. J.* (*Letters*), **252**, L11.
Kutner, M. L., Tucker, K. D., Chin, G., and Thaddeus, P. 1977, *Ap. J.*, **215**, 521.
Kutner, M. L., and Ulich, B. L. 1981, *Ap. J.*, **250**, 341.
Langer, W. 1976*a*, *Ap. J.*, **206**, 699.
———. 1976*b*, *Ap. J.*, **210**, 328.
Launay, J. M., and Roueff, E. 1977, *Astr. Ap.*, **56**, 289.
Loren, R. B., Plambeck, R. L., Davis, J. H., and Snell, R. L. 1981, *Ap. J.*, **245**, 495.
Mason, C. M., Lo, K. Y., Phillips, T. G., Sargent, A. I., Scoville, N. Z., and Woody, D. P. 1987, *Ap. J.*, **319**, 446.
Monteiro, T. S., and Flower, D. R. 1987, *M.N.R.A.S.*, **228**, 101.
Morris, M., Palmer, P., and Zuckerman, B. 1980, *Ap. J.*, **237**, 1.
Mufson, S. L., and Liszt, H. S. 1979, *Ap. J.*, **232**, 451.
Mundy, L. G., Evans, N. J., Snell, R. L., and Goldsmith, P. F. 1987, *Ap. J.*, **318**, 392.
Nadeau, D., Geballe, T. R., and Neugebauer, G. 1982, **253**, 154.
Nussbaumer, H. 1971, *Ap. J.*, **206**, 411.
Phillips, T. G., and Huggins, P. J. 1981, *Ap. J.*, **251**, 533.
Phillips, T. G., Huggins, P. J., Kuiper, T. B. H., and Miller, R. E. 1980, *Ap. J.* (*Letters*), **238**, L103.
Phillips, T. G., Knapp, G. R., Huggins, P. J., Werner, M. W., Wannier, P. G., Neugebauer, G., and Ennis, D. 1981, *Ap. J.*, **245**, 512.
Plambeck, R. L., Snell, R. L., and Loren, R. B. 1983, *Ap. J.*, **266**, 321.
Richardson, K. J., White, G. J., Avery, L. W., Lesurf, J. C. G., and Harten, R. H. 1985, *Ap. J.*, **290**, 637.
Saykally, R. J., and Evenson, K. M. 1980, *Ap. J.* (*Letters*), **238**, L107.
Schloerb, F. P., Snell, R. L., and Schwartz, P. R. 1987, *Ap. J.*, **319**, 426.
Scoville, N. Z., and Solomon, P. M. 1974, *Ap. J.* (*Letters*), **187**, L67.
Snell, R. L., Mundy, L. G., Goldsmith, P. F., Evans II, N. J., and Erickson, N. R. 1984*a*, *Ap. J.*, **276**, 625.
Snell, R. L., Scoville, N. Z., Sanders, D. B., and Erickson, N. R. 1984*b*, *Ap. J.*, **284**, 176.
Stacey, G. J. 1985, Ph.D. thesis, Cornell University.
Stutzki, J., Stacey, G. J., Genzel, R., Harris, A. I., Jaffe, D. T., and Lugten, J. B. 1988, *Ap. J.*, submitted.
Tarafdar, S. P., Prasad, S. S., Huntress, W. T. Jr., Villere, K. R., and Black, D. C. 1985, *Ap. J.*, **289**, 220.
Thronson Jr., H. A., and Lada, C. J. 1983, *Ap. J.*, **269**, 175.
Thronson Jr., H. A., Lada, C. J., Schwartz, P. R., Smith, H. A., Smith, J., Glaccum, W., Harper, D. A., and Loewenstein, R. C. 1984, *Ap. J.*, **280**, 154.
Tielens, A. G. G. M., and Hollenbach, D. 1985*a*, *Ap. J.*, **291**, 722.
———. 1985*b*, *Ap. J.*, **291**, 747.
Watson, D. M., Genzel, R., Townes, C. H., and Storey, J. W. V. 1985, *Ap. J.*, **298**, 316.
Werner, M. W., Becklin, E. E., Gatley, I., Neugebauer, G., Sellgren, K., Thronson Jr., H. A., Harper, D. A., Loewenstein, R., and Moseley, S. H. 1980, *Ap. J.*, **242**, 601.
Werner, M. W., Gatley, I., Harper, D. A., Becklin, E. E., Lowenstein, R. F., Telesco, C. M., and Thronson, H. A. 1976, *Ap. J.*, **204**, 420.
Williams, D. A., and Hartquist, T. W. 1984, *M.N.R.A.S.*, **210**, 141.
Zmuidzinas, J. 1987, Ph.D. thesis, University of California, Berkeley.
Zmuidzinas, J., Betz, A. L., and Goldhaber, D. M. 1986, *Ap. J.* (*Letters*), **307**, L75 (ZBG).

A. L. Betz, R. T. Boreiko, and D. M. Goldhaber: Space Sciences Laboratory, University of California, Berkeley, CA 94720

J. Zmuidzinas: Astronomy Department, University of Illinois, 1011 West Springfield Avenue, Urbana, IL 61801